Rate-dependent propagation of cardiac action potentials in a one-dimensional fiber

John W. Cain,[1,*] Elena G. Tolkacheva,[2] David G. Schaeffer,[1,4] and Daniel J. Gauthier[2,3,4]
[1]*Department of Mathematics, Duke University, Durham, North Carolina 27708, USA*
[2]*Department of Physics, Duke University, Durham, North Carolina 27708, USA*
[3]*Department of Biomedical Engineering, Duke University, Durham, North Carolina 27708, USA*
[4]*Center for Nonlinear and Complex Systems, Duke University, Durham, North Carolina 27708, USA*
(Received 19 July 2004; published 15 December 2004)

Action potential duration (APD) restitution, which relates APD to the preceding diastolic interval (DI), is a useful tool for predicting the onset of abnormal cardiac rhythms. However, it is known that different pacing protocols lead to different APD restitution curves (RCs). This phenomenon, known as APD rate dependence, is a consequence of memory in the tissue. In addition to APD restitution, conduction velocity restitution also plays an important role in the spatiotemporal dynamics of cardiac tissue. We present results concerning rate-dependent restitution in the velocity of propagating action potentials in a one-dimensional fiber. Our numerical simulations show that, independent of the amount of memory in the tissue, the wave-back velocity exhibits pronounced rate dependence and the wave-front velocity does not. Moreover, the discrepancy between wave-back velocity RCs is most significant for a small DI. We provide an analytical explanation of these results, using a system of coupled maps to relate the wave-front and wave-back velocities. Our calculations show that rate-dependent wave-back velocity can be present even if neither APD nor wave-front velocity exhibits rate dependence.

DOI: 10.1103/PhysRevE.70.061906 PACS number(s): 87.19.Hh, 05.45.−a, 87.10.+e

I. INTRODUCTION

When a cardiac cell is depolarized by an electrical stimulus, it exhibits a prolonged elevation of transmembrane potential known as an action potential. We define the action potential duration (APD) as the time required for the cell to achieve 80% repolarization following a depolarizing stimulus. The refractory period between the end of an action potential and the application of a subsequent stimulus is called the diastolic interval (DI). It is known that APD restitution (the dependence of the APD on preceding DI) is of fundamental importance in paced cardiac dynamics. In particular, studies [1,2] show that the slope of the APD restitution curve (RC) is linked to the onset of alternans, an abnormal cardiac rhythm characterized by long-short variation of APD, which may lead to ventricular fibrillation and sudden cardiac death [3–5].

Experimental [6–8] and analytical [9] investigations have shown that different pacing protocols lead to different APD RCs, a phenomenon sometimes[1] known as APD rate dependence. Several studies [10–12] indicate that the origin of APD rate dependence is the presence of memory in cardiac tissue. That is, the APD depends not only upon the preceding DI but also on the previous history of paced cardiac tissue. Memory appears to be a generic feature of cardiac muscle since it has been reported in humans [8] and various animals [7,13–15].

Testing for rate dependence involves the use of multiple pacing protocols and comparison of the resulting RCs. Two of the most commonly used pacing schemes are the dynamic and S1-S2 pacing protocols. Under the dynamic (steady-state) protocol, pacing is performed at a constant basic cycle length B until steady state is reached (no beat-to-beat variation in APD or DI). After recording the steady-state DI-APD pair, B is changed by an amount Δ and the process is repeated. The dynamic RC is constructed by plotting all steady-state DI-APD pairs obtained from the dynamic pacing protocol over a range of B values. The S1-S2 (standard) protocol also begins with pacing at a fixed basic cycle length B (S1 interval) until steady state is reached. Then, an S2 stimulus is applied at an interval B_1 after the final S1 stimulus. Setting $\delta = B_1 - B$, the S1-S2 RC is obtained by plotting the APD following the S2 stimulus versus the preceding DI for different values of δ. Note that there is only one dynamic RC, whereas each different S1 pacing interval can yield a distinct S1-S2 RC. For the purposes of this paper, we obtain only *local* S1-S2 RCs ($|\delta|$ small relative to S1) for different values of the S1 interval. In particular, following [16] we apply one short ($B_1 = B - \delta$) and one long ($B_1 = B + \delta$) perturbation at each different value of B.

The connection between rate-dependent APD restitution and memory is illustrated in Fig. 1, which shows APD RCs obtained from numerical simulations using two different ionic models (see Sec. II) of the cell membrane. Figure 1(a) is generated using a two-current model [17,18] with no memory: the dynamic and S1-S2 RCs are indistinguishable. Figure 1(b) is generated using a three-current ionic model [19,20] with some memory. One can see from Fig. 1(b) that segments of S1-S2 RCs (dashed curves) do not coincide with the dynamic RC (solid curve) for small DI values. The splitting between the dynamic and S1-S2 RCs is the manifestation of APD rate dependence.

Pacing the proximal end of a one-dimensional fiber of tissue results in a train of propagating action potentials. In

*Electronic mail: jcain@math.duke.edu

[1]As in [9,16], our use of the phrase *APD rate dependence* always refers to the dependence of the APD RC upon the pacing protocol, not the dependence of the APD upon the pacing rate.

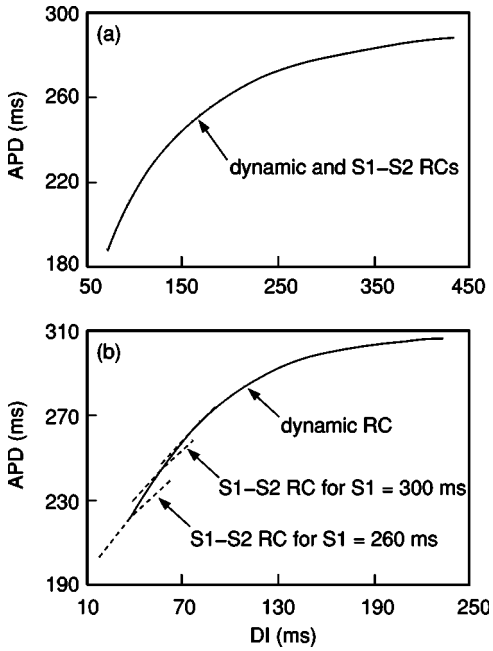

FIG. 1. Typical APD restitution curves obtained using dynamic and S1-S2 pacing protocols ($\Delta=40$ ms, $\delta=\pm 20$ ms) for two different ionic membrane models. (a) A two-current model. (b) A three-current model. The dynamic RC (solid) and local S1-S2 RCs (dashed) are shown for different values of S1.

this spatially extended setting, both the APD and the propagation speed of a pulse are influenced by the preceding pulse. Conduction-velocity restitution is analogous to APD restitution in that it relates the speed of an action potential at a given site to the DI at that site. Several authors [21–23] have noted that abrupt changes in the pacing rate lead to discrepancies between the wave-front and wave-back velocities. For this reason, we will always distinguish between wave-front (or activation front) velocity and wave-back (or recovery front) velocity of propagating action potentials.

In this paper, we investigate the rate dependence of wave-front and wave-back velocities of propagating action potentials in a one-dimensional fiber of cardiac cells. Using numerical simulations of different ionic membrane models (with and without memory) we demonstrate that the wave-back velocity exhibits pronounced rate dependence and the wave-front velocity does not (Sec. II). We derive an analytical relationship between wave-front and wave-back velocities by modeling cardiac dynamics using a system of coupled maps with an arbitrary amount of memory. We show that APD restitution, not memory, leads to wave-back velocity rate dependence (Sec. III). Consequently, rate-dependent wave-back velocity can be present even if neither APD nor wave-front velocity exhibits rate dependence. We provide conclusions and discussion in Sec. IV. An Appendix on the two-current ionic model is included for reference.

II. RATE-DEPENDENT VELOCITY: NUMERICAL RESULTS

Typically, the cardiac action potential is modeled by considering ionic currents that flow across the cell membrane via ion channels. The rate of change of the transmembrane voltage is obtained by summing all ionic currents and dividing by the membrane capacitance. The ion channels act as gates that regulate the permeabilities of ions, most notably sodium, potassium, and calcium. Hence, ionic models are presented as systems of ordinary differential equations that govern transmembrane voltage and gate variables.

In the case of a one-dimensional fiber, electrical coupling can be modeled by the inclusion of a diffusion term. The result is a reaction-diffusion partial differential equation known as the cable equation:

$$\frac{\partial v}{\partial t}=\kappa\frac{\partial^2 v}{\partial x^2}-\frac{I_{\text{total}}}{C_m},\quad 0\leqslant x\leqslant L, \tag{1}$$

where v denotes transmembrane voltage, x measures distance from the stimulus site, C_m is membrane capacitance, κ is a diffusion coefficient, and I_{total} is the sum of all ionic currents. The number of currents varies depending upon the complexity of the ionic model. The diffusion coefficient incorporates membrane capacitance, cell surface-to-volume ratio, and longitudinal resistivity of cardiac muscle tissue. In all of our numerical simulations $C_m=1\mu\text{F cm}^{-2}$ and $\kappa=0.001\text{ cm}^2\text{ ms}^{-1}$. Neumann boundary conditions $v_x(0,t)=v_x(L,t)=0$ are imposed at both ends of the cable.

To investigate rate-dependent propagation, we perform numerical simulations of Eq. (1). We apply both dynamic and S1-S2 pacing protocols at one end of a cable, and measure the wave-front and wave-back velocities of each propagating pulse. By analogy with APD rate dependence, velocity rate dependence means that different pacing protocols lead to different velocity RCs.

Since memory is responsible for APD rate dependence, it is natural to hypothesize that memory also leads to wave-front and wave-back velocity rate dependence. Consequently, we use two different ionic models in our numerical simulations: a two-current ionic model [18] with no memory and a three-current ionic model [20] with some memory.

The details of the numerical experiments are as follows. Using a cable of length $L=10$ cm, we solve Eq. (1) numerically with an operator-splitting method ($\Delta x=0.01$ cm, $\Delta t=0.01$ ms). Stimuli are applied over a 1 mm region at the proximal ($x=0$) end of the fiber using both the dynamic and S1-S2 protocols described in the Introduction. In all simulations, we use $\Delta=40$ ms and $\delta=\pm 20$ ms. Pacing results in a train of pulses that propagate left to right in the fiber. Measurements of DI, APD, wave-front speed, and wave-back speed are taken at $x=2.5$ cm. The position of a pulse wave front is defined as the x value for which the transmembrane voltage is -60 mV and $dv/dx<0$. Likewise, the wave-back position is defined as the x value at which $v=-60$ mV and $dv/dx>0$. Linear interpolation is used to improve tracking of wave-front and wave-back positions. Speeds are then computed by recording the time required for wave fronts and wave backs to traverse a 1-mm-wide interval centered at $x=2.5$ cm. For illustration purposes, Fig. 2 shows a projection of a solution of Eq. (1) (with two-current ionic model) onto the xt plane. The second and third action potentials obtained by pacing an initially quiescent fiber are shown. Different

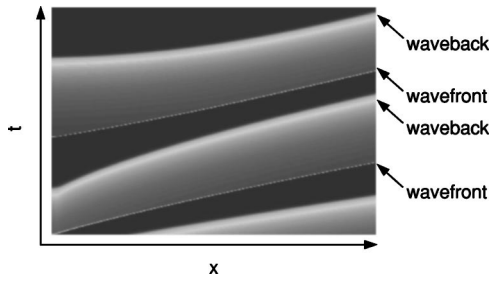

FIG. 2. Numerical solution of Eq. (1) with the two-current ionic model.

shades of gray correspond to different transmembrane voltages, with black corresponding to the rest potential. Note that projecting the wave fronts and wave backs onto the *xt* plane forms a sequence of curves.

Results of numerical simulations of Eq. (1) with the two-current ionic model (no memory) are presented in Fig. 3, which shows wave front [Fig. 3(a)] and wave back [Fig. 3(b)] velocity RCs. One can see from Fig. 3(a) that the wave-front velocity RCs resulting from different pacing protocols are indistinguishable. Thus, there is no significant rate dependence if velocities are measured at the wave front. However, one can see from Fig. 3(b) that segments of S1-S2 wave-back velocity RCs (dashed curves) do not coincide with the dynamic wave-back velocity RC (solid curve). As in the case of APD rate dependence (see Fig. 1), the splitting between wave-back velocity RCs is more pronounced for small values of DI.

Wave-front and wave-back velocity RCs obtained from numerical simulations of a cable with the three-current ionic model (that has some memory) are presented in Fig. 4. The

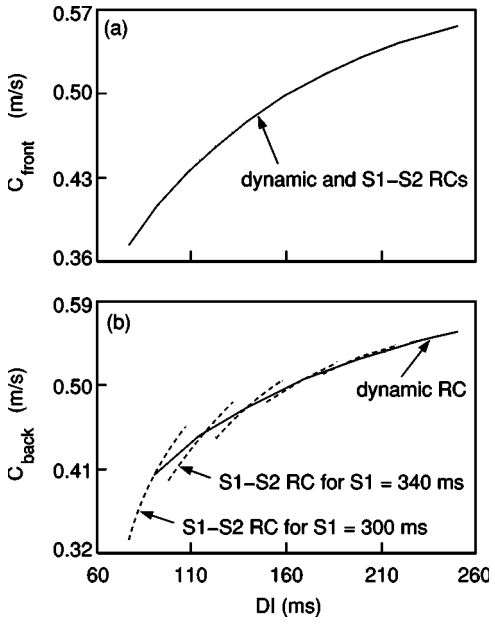

FIG. 3. Wave-front and wave-back velocity RCs obtained from numerical simulation of Eq. (1) with two-current ionic model ($\Delta = 40$ ms, $\delta = \pm 20$ ms). Velocities were measured at $x = 2.5$ cm. (a) Wave-front velocity RCs. (b) Wave-back velocity RCs. The dynamic RC is solid and the local S1-S2 RCs are dashed.

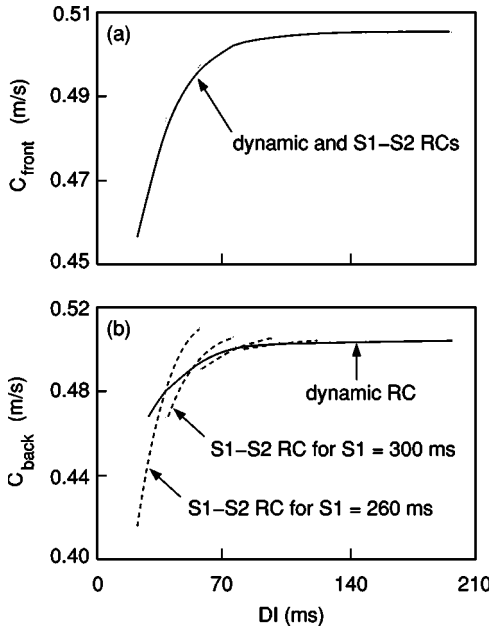

FIG. 4. Wave-front and wave-back velocity RCs obtained from numerical simulation of Eq. (1) with three-current ionic model ($\Delta = 40$ ms, $\delta = \pm 20$ ms). Velocities were measured at $x = 2.5$ cm. (a) Wave-front velocity RCs. (b) Wave-back velocity RCs. The dynamic RC is solid and the local S1-S2 RCs are dashed.

results are qualitatively similar to the two-current model results shown in Fig. 3.

There are two important points that we wish to emphasize. First, rate-dependent wave-back velocity restitution does not depend upon the presence of memory in the tissue, as evidenced by our two-current model simulations. Second, rate-dependent wave-back velocity is more pronounced for small values of DI. In what follows, we provide an analytical explanation of these findings.

III. RATE-DEPENDENT VELOCITY: ANALYTICAL RESULTS

In this section, we derive a relationship between wave-front and wave-back velocities. We approximate the dynamics of Eq. (1) using mappings instead of ionic models, an approach similar to [21,24–26]. Our analysis shows that wave-back velocity differs from wave-front velocity as a result of spatial variation in APD [see Eq. (8) below]. Hence, apart from the trivial case in which the APD RCs are constant, a rate-dependent wave-back velocity can exist even if the tissue lacks both memory and rate-dependent wave-front velocity.

Mapping models that express the APD in terms of preceding DI and APD values have been employed by many authors [1,11,12,20,27] to describe local tissue dynamics. For example, based on experiments with frog tissue, Nolasco and Dahlen [1] proposed a simple mapping model of the form

$$A_{n+1} = F(D_n), \tag{2}$$

where A_n and D_n denote the nth APD and DI values, respectively. Using asymptotics, Mitchell and Schaeffer [18] derive

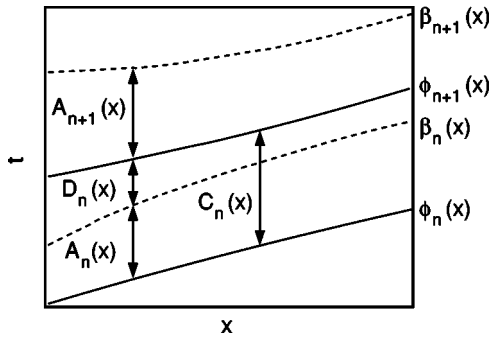

FIG. 5. Schematic representation of the wave fronts (solid curves) and wave backs (dashed curves) in Fig. 2.

a mapping of the form (2) from the governing equations of a two-current ionic model. A similar analysis by Tolkacheva *et al.* [20] shows that the three-current Fenton-Karma ionic model [19] leads to a mapping with two arguments:

$$A_{n+1} = F(A_n, D_n). \tag{3}$$

In general, the number of arguments of F determines how much memory is present. The mapping model (2) has no memory, and all APD RCs coincide as in Fig. 1(a). The mapping model (3) has some memory, and the dynamic and S1-S2 RCs are different as in Fig. 1(b). Below, we consider mappings in which F has many arguments.

We now generalize mapping models appropriate for a patch to the case of one-dimensional fibers. In what follows, we assume that wave backs are not greatly affected by electrotonic coupling so that repolarization is driven by local effects only. That is, using the terminology of [28,29], we consider phase wave backs as opposed to triggered wave backs. This assumption allows us to apply a mapping locally at each x along the fiber [see Eq. (4) below].

We represent the wave fronts and wave backs in solutions of Eq. (1) schematically. Refer to Fig. 5, which shows the projection of a particular level set of the surface in Fig. 2 onto the xt plane. The curves in Fig. 5 are identified with the sequence of wave fronts and wave backs. We define $\phi_n(x)$ $[\beta_n(x)]$ as the time at which the nth wave front (wave back) reaches x.

Let us assume that, at each x along the fiber, the APD can be represented as a function of an arbitrary number of preceding APDs and DIs in the form

$$A_{n+1}(x) = F(\mathbf{A}_n(x), \mathbf{D}_n(x)), \tag{4}$$

i.e., an arbitrary amount of memory is included. Here,

$$\mathbf{A}_n(x) = (A_n(x), A_{n-1}(x), \ldots, A_{n+1-m}(x)), \tag{5}$$

$$\mathbf{D}_n(x) = (D_n(x), D_{n-1}(x), \ldots, D_{n+1-k}(x)),$$

and $m \geqslant 0$ and $k \geqslant 1$ are integers characterizing how many preceding states are taken into account in the mapping model. Since many previous states are involved, Eq. (4) makes sense only for $m, k \leqslant n$. Note that $m=0$, $k=1$ corresponds to the simplest mapping model Eq. (2), the case of no memory. The case $m=1$, $k=1$ corresponds to a mapping of the form of Eq. (3) with some memory.

Let us also assume that the velocity of the $(n+1)$st wave front, $c_{\text{front}}(\mathbf{A}_n(x), \mathbf{D}_n(x))$, depends upon preceding (local) APD and DI values. This velocity is computed by inverting the slope of $\phi_{n+1}(x)$:

$$\frac{d\phi_{n+1}(x)}{dx} = \frac{1}{c_{\text{front}}(\mathbf{A}_n(x), \mathbf{D}_n(x))} \equiv G(\mathbf{A}_n(x), \mathbf{D}_n(x)). \tag{6}$$

Using the above framework, the wave-back velocity c_{back} is completely determined by the wave-front velocity. Referring to Fig. 5, note that

$$\beta_{n+1}(x) = \phi_{n+1}(x) + A_{n+1}(x). \tag{7}$$

Differentiating Eq. (7) with respect to x yields a relationship between wave-front and wave-back velocities. Simply stated,

$$\frac{1}{c_{\text{back}}} = \frac{1}{c_{\text{front}}} + A'_{n+1}(x), \tag{8}$$

which shows that the wave-back velocity is the same as the wave-front velocity modified by the spatial variation in the APD. Assuming that the APD RCs are nonconstant, it follows that even in the absence of both memory and rate-dependent wave-front velocity, the fiber can still exhibit rate-dependent wave-back velocity. To make Eq. (8) more explicit, we now compare wave-front and wave-back velocities for both the dynamic and S1-S2 protocols.

A. Dynamic pacing protocol

Under the dynamic pacing protocol, pacing is performed at a constant basic cycle length B at $x=0$ until steady state is reached. In what follows, we assume that a 1:1 steady-state response results from dynamic pacing. That is, every stimulus produces an action potential and there is no beat-to-beat variation in the APD or DI. Note that $\phi_n(x)$ and $\beta_n(x)$ are parallel[2] lines in the xt plane if a 1:1 steady state is reached.

When steady state is reached, the vectors $\mathbf{A}_n(x)$ and $\mathbf{D}_n(x)$ are constant:

$$\mathbf{A}_n(x) = \mathbf{A}^* \equiv (A^*, A^*, \ldots A^*), \tag{9}$$

$$\mathbf{D}_n(x) = \mathbf{D}^* \equiv (D^*, D^*, \ldots D^*),$$

and $(\mathbf{A}^*, \mathbf{D}^*)$ is the fixed point of Eq. (4). Plotting $c_{\text{front}}(\mathbf{A}^*, \mathbf{D}^*)$ versus D^*, we obtain a point on the dynamic wave-front velocity RC. The curves $\beta_{n+1}(x)$ and $\phi_{n+1}(x)$ have the same slope since they are parallel at steady state: $\beta_{n+1}(x) = \phi_{n+1}(x) + A^*$. Therefore, since there is no spatial variation in the APD, the dynamic wave-back and wave-front velocity RCs are identical. Hence, from now on we refer to *the* dynamic velocity RC and use the notation $c_{\text{dyn}} = c_{\text{dyn}}(D^*)$.

Defining the cycle length as

[2] In the ordinary differential equations derived in Sec. III, pacing is applied at the $x=0$ boundary, not over a small interval $[0, \epsilon]$. Therefore, in steady state, the wave fronts and wave backs really are straight lines.

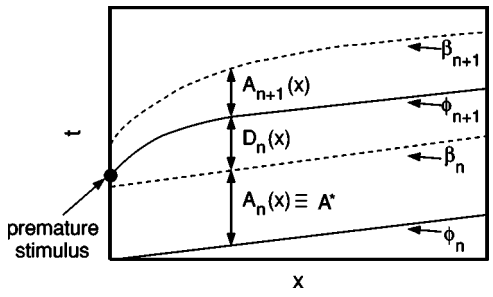

FIG. 6. Deflection of the $(n+1)$st wave front and wave back due to a premature $(B_1<B)$ S2 stimulus. The shortened diastolic interval at the stimulus site slows the propagation speed. Solid curves represent wave fronts and dashed curves represent wave backs.

$$C_n(x) = A_n(x) + D_n(x) = \phi_{n+1}(x) - \phi_n(x), \tag{10}$$

it follows from Eq. (6) that

$$\frac{d}{dx}C_n(x) = G(\mathbf{A}_n(x),\mathbf{D}_n(x)) - G(\mathbf{A}_{n-1}(x),\mathbf{D}_{n-1}(x)). \tag{11}$$

According to Eqs. (10) and (4), the cycle length also satisfies the algebraic condition

$$C_n(x) = F(\mathbf{A}_{n-1}(x),\mathbf{D}_{n-1}(x)) + D_n(x), \tag{12}$$

and thus Eqs. (11) and (12) imply that

$$\frac{d}{dx}[F(\mathbf{A}_{n-1}(x),\mathbf{D}_{n-1}(x)) + D_n(x)] = G(\mathbf{A}_n(x),\mathbf{D}_n(x)) - G(\mathbf{A}_{n-1}(x),\mathbf{D}_{n-1}(x)). \tag{13}$$

Since $C_n(0)=B$ for all n under the dynamic pacing protocol, we obtain the following boundary condition at $x=0$:

$$D_n(0) = B - F(\mathbf{A}_{n-1}(0),\mathbf{D}_{n-1}(0)). \tag{14}$$

The sequence of equations Eq. (13) can be solved iteratively to construct a diagram similar to Fig. 5. If the vectors of functions $\mathbf{A}_n(x)$ and $\mathbf{D}_{n-1}(x)$ are known, we can solve Eq. (13) to determine $D_n(x)$. Note that $A_{n+1}(x)$ can then be computed by applying Eq. (4).

B. S1-S2 pacing protocol

In the S1-S2 protocol, tissue is paced at a basic cycle length B until steady state is reached. Then, an S2 stimulus is introduced at an interval $B_1=B\pm\delta$ following the last S1 stimulus and the response to the S2 stimulus is measured. In what follows, we assume that the S2 stimulus is applied prematurely $(B_1=B-\delta)$ following a train of n S1 stimuli. The S2 stimulus causes a deflection in the $(n+1)$st wave front and wave back as shown in Fig. 6.

These assumptions imply that

$$\mathbf{A}_n(x) = \mathbf{A}^*, \tag{15}$$

$$\mathbf{D}_n(x) = (D_n(x), D^*, \ldots, D^*),$$

and yield the boundary condition

$$D_n(0) = B_1 - A^*. \tag{16}$$

Equation (13) reduces to

$$\frac{dD_n(x)}{dx} = G(\mathbf{A}^*,\mathbf{D}_n(x)) - G^*, \tag{17}$$

where $G^*=G(\mathbf{A}^*,\mathbf{D}^*)=c_{\mathrm{dyn}}^{-1}$. Linearizing Eq. (17) about the point $(\mathbf{A}^*,\mathbf{D}^*)$, we have

$$\frac{dD_n(x)}{dx} = -\lambda[D_n(x) - D^*], \tag{18}$$

where

$$\lambda = -\left.\frac{\partial G}{\partial D_n}\right|_{(\mathbf{A}^*,\mathbf{D}^*)}. \tag{19}$$

Since c_{front} typically depends monotonically on the argument D_n [see Fig. 3(a)], it is natural to assume that $\lambda>0$. The solution of Eq. (18) with the boundary condition (16) is

$$D_n(x) = D^* - \delta e^{-\lambda x}. \tag{20}$$

Let $c_{\mathrm{front}}^{S_{12}}$ and $c_{\mathrm{back}}^{S_{12}}$ denote the wave-front and wave-back velocities of the action potential generated by the S2 stimulus. In order to compute $c_{\mathrm{front}}^{S_{12}}$, observe that (see Fig. 6)

$$\phi_{n+1}(x) = \beta_n(x) + D_n(x). \tag{21}$$

We know that $\phi_n(x)$ and $\beta_n(x)$ are parallel since they represent the wave front and wave back associated with the final S1 stimulus. Therefore, $d\beta_n/dx=d\phi_n/dx=G^*$, and differentiating Eq. (21) with respect to x gives

$$c_{\mathrm{front}}^{S_{12}} = \frac{1}{G^* + \delta\lambda e^{-\lambda x}}. \tag{22}$$

According to Eq. (15), the only nonconstant argument of the function F is $D_n(x)$. Therefore, differentiating Eq. (7) with respect to x gives

$$\frac{d\beta_{n+1}}{dx} = \frac{d\phi_{n+1}}{dx} + \frac{\partial F}{\partial D_n}\frac{dD_n}{dx} = G^* + \delta\lambda e^{-\lambda x}\left(1 + \frac{\partial F}{\partial D_n}\right), \tag{23}$$

which implies that

$$c_{\mathrm{back}}^{S_{12}} = \frac{1}{G^* + \delta\lambda e^{-\lambda x}(1 + \partial F/\partial D_n)}. \tag{24}$$

The partial derivative $\partial F/\partial D_n$ in Eq. (24) is evaluated at $(\mathbf{A}^*, D^*-\delta e^{-\lambda x}, D^*, \ldots, D^*)$. Equations (22) and (24) are analytical expressions for the wave-front and wave-back velocity for the S1-S2 pacing protocol.

Comparing Eqs. (22) and (24) again demonstrates that APD restitution, not memory, is responsible for the rate dependence we study here. Indeed, the only difference between expressions (22) and (24) is the presence of the multiplier $(1+\partial F/\partial D_n)$ in the formula for the wave-back velocity. The partial derivative $\partial F/\partial D_n$ in Eq. (24) represents the slope S_{12} of the S1-S2 APD RC as demonstrated in [9]. As the DI decreases, S_{12} typically increases, thereby increasing the discrepancy between the wave-front and wave-back velocities.

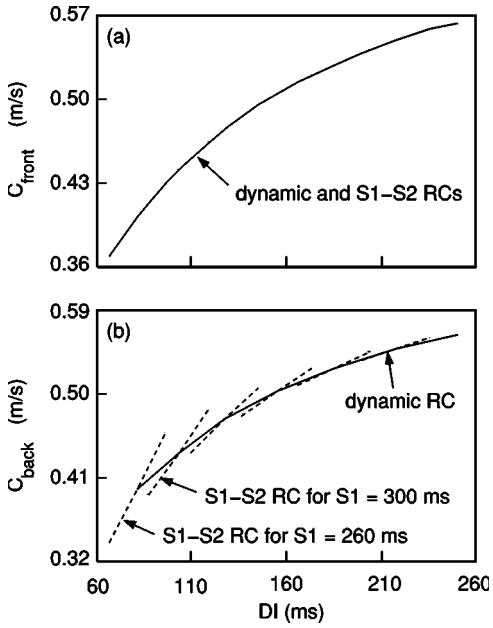

FIG. 7. Wave-front and wave-back velocity RCs generated using Eqs. (22), (24), (A3), and (A9) ($\Delta=40$ ms, $\delta=\pm 20$ ms). Velocities were measured at $x=2.5$ cm. (a) Wave-front velocity RCs: the dynamic and S1-S2 curves appear to coincide. (b) Wave-back velocity RCs: the dynamic curve is solid and local S1-S2 curves are dashed.

Finally, regardless of how much memory is included in the mapping model, Eqs. (22) and (24) depend upon $D_n(x)$ and no other preceding states.

C. An example: Rate-dependent velocity (9)and the two-current model

In this subsection, we explain how to apply Eqs. (22) and (24), using the two-current model as an example. Both Eqs. (22) and (24) require that we know formulas for the dynamic velocity RC (since $G^*=c_{\rm dyn}^{-1}$) and the function F. Leading-order expressions for F and $c_{\rm dyn}$ can be derived analytically for the two-current model (see the Appendix).

The dynamic velocity RC is provided by Eq. (A9). Combining Eqs. (22) and (A9), we generate all S1-S2 wave-front velocity RCs. Likewise, combining Eqs. (24), (A3), and (A9) allows us to construct all S1-S2 wave-back velocity RCs.

All of the analytically derived RCs are shown in Fig. 7. Figure 7(a) shows all wave-front velocity RCs. The dynamic and S1-S2 wave-front velocity RCs are indistinguishable. The wave-back velocity RCs are shown in Fig. 7(b). Note the presence of rate dependence, as evidenced by the splitting of the dynamic (solid) and S1-S2 (dashed) RCs. We remark that Fig. 7 shows excellent quantitative agreement with the results of numerical simulations shown in Fig. 3.

IV. CONCLUSIONS

We have demonstrated that a rate-dependent wave-back velocity can exist even in the absence of both memory and rate-dependent wave-front velocity. Our numerical simulations show that both the two- and three-current models exhibit rate-dependent wave-back velocity, whereas neither model exhibits rate-dependent wave-front velocity. The fact that even a memoryless two-current model that lacks rate-dependent wave-front velocity still exhibits rate-dependent wave-back velocity seems surprising at first. To explain this phenomenon analytically, using an approach similar to that of [21,24–26], we derive a relationship between the wave-front and wave-back speeds. Although the dynamic wave-front and wave-back velocity RCs are identical, the fact that Eqs. (22) and (24) differ shows that S1-S2 velocity RCs need not coincide. Therefore, if the wave-front (wave-back) velocity lacks rate dependence, then the wave-back (wave-front) velocity must exhibit rate dependence. The magnitude of the term $(1+\partial F/\partial D_n)$ in Eq. (24) determines the difference between the S1-S2 wave-front and wave-back velocities. Since the partial derivative $S_{12}=\partial F/\partial D_n$ represents the slope of an S1-S2 APD RC, the greatest discrepancy between the wave-front and wave-back velocities should occur at small DI (where S_{12} is greatest). This prediction is consistent with the results of our numerical simulations (Figs. 3 and 4).

ACKNOWLEDGMENTS

We gratefully acknowledge the financial support of the National Science Foundation through Grants No. PHY-0243584 and No. DMS-9983320 and the National Institutes of Health through Grant No. 1R01-HL-72831.

APPENDIX

A detailed analysis of the two-current model equations appears in [18]. With the two-current model, Eq. (1) reads

$$\frac{\partial v}{\partial t}=\kappa\frac{\partial^2 v}{\partial x^2}+\frac{h}{\tau_{\rm in}}v^2(1-v)-\frac{v}{\tau_{\rm out}}, \tag{A1}$$

$$\frac{dh}{dt}=\begin{cases}\dfrac{1-h}{\tau_{\rm open}}, & v<v_{\rm crit},\\[2ex] -\dfrac{h}{\tau_{\rm close}}, & v>v_{\rm crit},\end{cases} \tag{A2}$$

where v is the transmembrane voltage (scaled to range between 0 and 1) and h is a gate variable. The parameters $\tau_{\rm in}$, $\tau_{\rm close}$, $\tau_{\rm out}$, and $\tau_{\rm open}$ are time constants associated with different phases of the action potential. The gate opens or closes according to whether v exceeds the threshold voltage $v_{\rm crit}$. Typical choices for the time constants and critical voltage are $\tau_{\rm in}=0.1$ ms, $\tau_{\rm out}=2.4$ ms, $\tau_{\rm open}=130$ ms, $\tau_{\rm close}=150$ ms, and $v_{\rm crit}=0.13$.

A leading-order estimate of the APD RC is derived in [18]. If the time constants satisfy an asymptotic condition $\tau_{\rm in}\ll\tau_{\rm out}\ll\tau_{\rm open},\tau_{\rm close}$, then

$$A_{n+1}=F(D_n)=\tau_{\rm close}\ln\left(\frac{h_s(D_n)}{h_{\rm min}}\right) \tag{A3}$$

to leading order, where

$$h_s(D_n) = 1 - (1 - h_{\min})e^{-D_n/\tau_{\text{open}}}, \tag{A4}$$

and $h_{\min} = 4\tau_{\text{in}}/\tau_{\text{out}}$.

To derive a leading-order estimate of c_{dyn}, we follow Murray [30]. Assume the fiber is paced at a constant basic cycle length until steady state is reached so that all pulses propagate with speed $c_{\text{dyn}} = c_{\text{dyn}}(D^*)$. We seek traveling wave train solutions to Eq. (A1). In the neighborhood of a wave front, introduce the coordinate

$$\xi = \frac{1}{\tau_{\text{in}}}\left(t + \frac{x}{c_{\text{dyn}}}\right), \tag{A5}$$

where the speed c_{dyn} is to be determined. Assume that $v(x,t) = V(\xi)$ and $h(x,t) = H(\xi)$. Since τ_{in} is small relative to the time constants in Eq. (A2), we may safely approximate the value of h by a constant in the narrow wave-front region: $h \approx h^* \equiv h_s(D^*)$. Inserting $v(x,t) = V(\xi)$ into Eq. (A1), we obtain an ordinary differential equation

$$\frac{\kappa}{c_{\text{dyn}}^2 \tau_{\text{in}}} V'' - V' + h^* V(V_- - V)(V - V_+) = 0, \tag{A6}$$

where the primes denote differentiation with respect to ξ and

$$V_\pm = \frac{1}{2}\left(1 \pm \sqrt{1 - \frac{h_{\min}}{h^*}}\right). \tag{A7}$$

We remark that V_- is an unstable equilibrium of Eq. (A6) corresponding to the threshold for excitation, and V_+ is an unstable equilibrium associated with the excited state. We seek solutions to Eq. (A6) such that $V(\xi) \to 0$ as $\xi \to -\infty$ and $V(\xi) \to V_+$ as $\xi \to \infty$. It is possible to find a solution of a simpler differential equation

$$V' = -aV(V - V_+) \tag{A8}$$

that also satisfies Eq. (A6) for unique values of the constant a and the speed c_{dyn}. Substituting (A8) into Eq. (A6), one finds that

$$c_{\text{dyn}} = \left(\frac{1}{2}V_+ - V_-\right)\sqrt{\frac{2\kappa h^*}{\tau_{\text{in}}}}. \tag{A9}$$

[1] J. B. Nolasco and R. W. Dahlen, J. Appl. Physiol. **25**, 191 (1968).
[2] M. R. Guevara, G. Ward, A. Shier and L. Glass, in *Proceedings of the 11th Computers in Cardiology Conference* (IEEE Computer Society, Los Angeles, 1984), p. 167.
[3] A. Karma, Chaos **4**, 461 (1994).
[4] D. Rosenbaum, L. Jackson, J. Smith, H. Garan, J. Ruskin, and R. Cohen, N. Engl. J. Med. **330**, 235 (1994).
[5] M. Watanabe, N. F. Otani, and R. F. Gilmour, Jr., Circ. Res. **76**, 915 (1995).
[6] M. R. Boyett and B. R. Jewell, J. Physiol. (London) **285**, 359 (1978).
[7] V. Elharrar and B. Surawicz, Am. J. Physiol. **244**, H782 (1983).
[8] M. R. Franz, C. D. Swerdlow, L. B. Liem, and J. Schaefer, J. Clin. Invest. **82**, 972 (1988).
[9] E. G. Tolkacheva, D. G. Schaeffer, D. J. Gauthier, and W. Krassowska, Phys. Rev. E **67**, 031904 (2003).
[10] R. M. Gulrajani, IEEE Comp. Cardiol. 244, 629 (1987).
[11] D. R. Chialvo, D. C. Michaels, and J. Jalife, Circ. Res. **66**, 525 (1990).
[12] N. F. Otani and R. F. Gilmour, Jr., J. Theor. Biol. **187**, 409 (1997).
[13] G. M. Hall, S. Bahar, and D. J. Gauthier, Phys. Rev. Lett. **82**, 2995 (1999).
[14] L. S. Gettes, G. N. Morehouse, and B. Surawicz, Circ. Res. **30**, 55 (1972).
[15] C. L. Gibbs and E. A. Johnson, Circ. Res. **9**, 165 (1961).
[16] S. S. Kalb, H. M. Dobrovolny, E. G. Tolkacheva, S. F. Idriss, W. Krassowska, and D. J. Gauthier, J. Cardiovasc. Electrophysiol. **15**, 698 (2004).
[17] A. Karma, Phys. Rev. Lett. **71**, 1103 (1993).
[18] C. C. Mitchell and D. G. Schaeffer, Bull. Math. Biol. **65**, 767 (2003).
[19] F. H. Fenton and A. Karma, Chaos **8**, 20 (1998).
[20] E. G. Tolkacheva, D. G. Schaeffer, D. J. Gauthier, and C. C. Mitchell, Chaos **12**, 1034 (2002).
[21] M. Courtemanche, J. P. Keener, and L. Glass, SIAM (Soc. Ind. Appl. Math.) J. Appl. Math. **56**, 119 (1996).
[22] M. Courtemanche, Chaos **6**, 579 (1996).
[23] F. H. Fenton, E. M. Cherry, H. M. Hastings, and S. J. Evans, Chaos **12**, 852 (2002).
[24] M. A. Watanabe, F. H. Fenton, S. J. Evans, H. M. Hastings, and A. Karma, J. Cardiovasc. Electrophysiol. **12**, 196 (2001).
[25] J. J. Fox, R. F. Gilmour, and E. Bodenschatz, Phys. Rev. Lett. **89**, 198101 (2002).
[26] B. Echebarria and A. Karma, Phys. Rev. Lett. **88**, 208101 (2002).
[27] J. J. Fox, E. Bodenschatz, and R. F. Gilmour, Phys. Rev. Lett. **89**, 138101 (2002).
[28] J. J. Tyson and J. P. Keener, Physica D **32**, 327 (1988).
[29] E. Cytrynbaum and J. P. Keener, Chaos **12**, 788 (2002).
[30] J. D. Murray, *Mathematical Biology* (Springer, Berlin, 1993).